ARTICLE

doi:10.1038/nature09559

Encoding of conditioned fear in central amygdala inhibitory circuits

Stephane Ciocchi[1]*, Cyril Herry[1]*†, François Grenier[1], Steffen B. E. Wolff[1], Johannes J. Letzkus[1], Ioannis Vlachos[2], Ingrid Ehrlich[1]†, Rolf Sprengel[3], Karl Deisseroth[4], Michael B. Stadler[1], Christian Müller[1] & Andreas Lüthi[1]

The central amygdala (CEA), a nucleus predominantly composed of GABAergic inhibitory neurons, is essential for fear conditioning. How the acquisition and expression of conditioned fear are encoded within CEA inhibitory circuits is not understood. Using *in vivo* electrophysiological, optogenetic and pharmacological approaches in mice, we show that neuronal activity in the lateral subdivision of the central amygdala (CEl) is required for fear acquisition, whereas conditioned fear responses are driven by output neurons in the medial subdivision (CEm). Functional circuit analysis revealed that inhibitory CEA microcircuits are highly organized and that cell-type-specific plasticity of phasic and tonic activity in the CEl to CEm pathway may gate fear expression and regulate fear generalization. Our results define the functional architecture of CEA microcircuits and their role in the acquisition and regulation of conditioned fear behaviour.

The amygdala is a key brain structure involved in the acquisition and expression of conditioned fear responses[1–3]. In the classical circuit model of fear conditioning, the lateral nucleus of the amygdala is thought of as the primary site where associations between the conditioned stimulus (CS) and the unconditioned stimulus (US) are formed and stored[1–5]. In contrast to the lateral nucleus of the amygdala (LA), the central nucleus of the amygdala (CEA) has been considered to be primarily involved in the behavioural expression of conditioned fear responses. CEA output neurons, most of which are located in its medial subdivision (CEm), project to downstream targets in the brainstem and in the hypothalamus where they orchestrate conditioned autonomic and motor responses[6–8]. It is still unclear whether conditioned fear responses are triggered by activation or inhibition of these output neurons. Experiments involving lesions, pharmacological manipulations and electrical stimulation indicate that the activity of CEm output neurons drives conditioned fear responses[2]; however, the only *in vivo* recordings from identified CEA output neurons indicate the opposite[9].

Recent evidence also supports a role of the CEA in the learning process itself. Acute and reversible inactivation of the CEA during fear conditioning, or local blockade of NMDA (*N*-methyl-D-aspartate) receptors, result in impaired acquisition of conditioned fear responses[10,11]. This strongly indicates that activity-dependent plasticity within the CEA is necessary for the acquisition of fear conditioning[12,13]. Because CEm output neurons are under tight inhibitory control from the lateral and capsular subdivisions (together referred to as CEl)[14–17], a reduction in CEl to CEm inhibition might contribute to increased CEm output after fear conditioning. Although this scenario is indirectly supported by the observation that enhancing inhibitory activity in CEl by endogenous neuropeptides and exogenous substances, such as ethanol, has anxiolytic effects[18], the role of the intra-CEA inhibitory circuitry in the acquisition and expression of conditioned fear responses is not known.

Differential role of CEl and CEm

To test the impact of neuronal activity in CEm on freezing behaviour, we selectively activated or inhibited CEm neurons using optogenetic and pharmacological approaches. Activation of CEm neurons was achieved by bilateral targeted injection of a virus expressing channelrhodopsin-2 (ChR2) in neurons[19,20] (Fig. 1a, b and Supplementary Fig. 1). In freely moving animals, bilateral activation of CEm induced strong and reversible freezing responses (Fig. 1c).

Conversely, we used microiontophoresis of a fluorescently labelled $GABA_A$ receptor agonist[21] (muscimol-bodipy (BPY)) to inhibit neuronal activity in a targeted and reversible manner (Fig. 1d). Bilateral inactivation of CEm, or of the entire CEA (CEm and CEl), did not elicit freezing behaviour (Fig. 1e). In contrast, inactivation of CEl alone induced unconditioned freezing (Fig. 1e). These results indicate that neuronal activity in CEm is necessary and sufficient for driving freezing behaviour, and that CEm is under tonic inhibitory control from CEl.

We next examined the contribution of distinct CEA subnuclei to the acquisition of conditioned freezing. Mice were trained in a discriminative fear conditioning paradigm (see Methods). Twenty-four hours after conditioning, mice exhibited freezing behaviour upon presentation of the conditioned stimulus (CS^+; $P < 0.001$ versus pre-conditioning baseline). Consistent with a previous study[11], targeted bilateral inactivation of the entire CEA during fear conditioning resulted in a profound memory deficit when measured 24 h later in the absence of muscimol-BPY (Fig. 1f). A comparable memory deficit was observed after inactivation of CEl, but not of CEm (Fig. 1f). Notably, inactivation of CEA or CEl did not impair US detection, and after wash-out of muscimol-BPY, animals could be fear conditioned, indicating that muscimol-BPY did not cause irreversible damage (Supplementary Fig. 2).

We next examined the role of CEl and CEm for memory retrieval or expression by local application of muscimol-BPY 24 h after conditioning (Fig. 1g). In contrast to the acquisition phase, we found that whereas inactivation of the entire CEA or CEm resulted in a retrieval/expression deficit, inactivation of CEl did not reduce conditioned freezing levels, although occlusion by unconditioned freezing is possible (Fig. 1g and Supplementary Fig. 3). Together, these data indicate a functional dissociation of CEl and CEm during the acquisition and expression of conditioned fear responses, and indicate a role for activity-dependent neuronal plasticity in CEl in acquisition.

[1]Friedrich Miescher Institute for Biomedical Research, Maulbeerstrasse 66, 4058 Basel, Switzerland. [2]Bernstein Center for Computational Neuroscience, 79104 Freiburg, Germany. [3]Department of Molecular Neurobiology, Max Planck Institute for Medical Research, Jahnstrasse 29, 69120 Heidelberg, Germany. [4]Department of Bioengineering, Stanford University, Stanford, California 94305, USA. †Present addresses: INSERM U862, Neurocentre Magendie, 146 Rue Léo-Saignat, 33077 Bordeaux, France (C.H.); Hertie Institute for Clinical Brain Research, 72076 Tübingen, Germany (I.E.). *These authors contributed equally to this work.

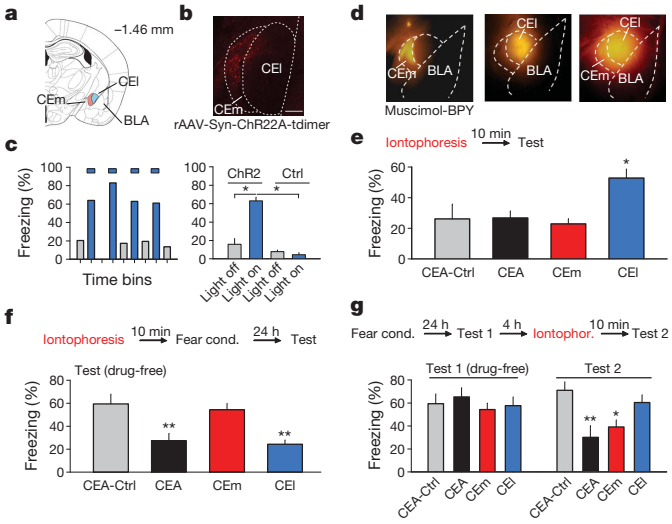

Figure 1 | Differential role of CEl and CEm in fear expression and acquisition. **a**, Coronal section of the mouse brain indicating the location of the central amygdala (CEA). CEl/CEm, lateral/medial subdivisions of CEA. Numbers indicate the antero-posterior coordinates caudal to bregma. **b**, Red fluorescent neurons in CEm infected with AAV-ChR22A-tdimer. Scale bar, 100 μm. **c**, Left: example experiment illustrating rapid and reversible freezing induced by bilateral stimulation of ChR2-expressing CEm neurons with 10 s of blue light (inter-stimulation intervals, 30–60 s). Right: summary data demonstrating significant light-induced freezing responses in AAV-ChR22A-tdimer infected animals, but not in sham-operated controls. **d**, Epifluorescence image illustrating microiontophoretic application of fluorescently labelled muscimol (muscimol-BPY) targeted at CEm, CEl, or the entire CEA. **e**, Top: experimental protocol. Bottom: inactivation of CEl induced unconditioned freezing. Inactivation of CEm, or the entire CEA, had no effect on freezing. Control mice received BPY only. **f**, Top: muscimol-BPY was applied during fear conditioning. Animals were tested drug-free 24 h later. Bottom: compared with animals injected with BPY only, inactivation of CEl or CEA, but not of CEm, prevented fear acquisition. **g**, Top: animals were fear conditioned in the absence of muscimol-BPY and tested 24 h later. Muscimol-BPY was applied before animals were re-tested on the same day. Bottom left: at test, all experimental groups exhibited equal freezing levels before muscimol application. Bottom right: compared with animals injected with BPY only, inactivation of CEm or CEA, but not CEl, impaired fear expression. All error bars indicate mean ± s.e.m. $*P < 0.05$, $**P < 0.01$. Statistical analysis is shown in the Supplementary Information.

Organization of CEA inhibitory networks

Next, we investigated fear-conditioning-induced changes in CS-evoked neuronal firing in the CEl. Mice were implanted with chronic recording electrodes and 167 units located in the CEl were recorded (Supplementary Fig. 4). Two classes of CEl units exhibiting opposite changes in CS-evoked activity after fear conditioning were revealed by comparing *z*-scored CS responses 24 h after conditioning to baseline levels measured during habituation. Whereas 30% of units acquired an excitatory response (CEl_{on} neurons) (Fig. 2a), 25% of CEl neurons displayed a strong inhibitory response to the CS^+ after fear conditioning (CEl_{off} neurons) (Fig. 2b). The rest of the units (45%) did not exhibit any tone-evoked responses. Changes in CS^+-evoked responses were already detectable during fear conditioning, and in animals exhibiting behavioural discrimination, both CEl_{on} and CEl_{off} units exhibited discriminating neuronal responses (Supplementary Fig. 4). Thus, fear conditioning induces rapid, specific and persistent changes in CS-evoked activity of CEl neurons.

The inverse direction of fear-conditioning-induced plasticity in CEl_{on} and CEl_{off} neurons indicated the possibility that inhibitory responses of CEl_{off} neurons were mediated by local inputs from CEl_{on} neurons. Latency analysis of CS responses in CEl_{on} and CEl_{off} neurons revealed that CS-evoked excitation in CEl_{on} neurons started before CEl_{off} neurons were inhibited (Supplementary Fig. 4). The short onset latency of CS-evoked excitation in CEl_{on} neurons (<15 ms) indicates that they may, like CEm neurons[22,23], receive direct input from sensory thalamus[24]. Cross-correlating spontaneously occurring spikes of simultaneously recorded CEl_{on} and CEl_{off} neurons revealed substantial, yet asymmetrical, short-latency inhibitory interactions between the two classes of neurons (Fig. 2c, f; CEl_{on} to CEl_{off}, 9 of 35 pairs; CEl_{off} to CEl_{on}, 3 of 35 pairs; $P < 0.05$, binomial test). Inhibitory cross-correlations among CEl_{on} neurons (0 of 22 possible connections) or among CEl_{off} neurons (2 of 54 possible connections) were rare. Thus, fear conditioning leads to a shift in the balance of activity between distinct functional classes of CEl neurons embedded into highly organized local inhibitory circuits.

On the basis of previous anatomical and *in vitro* electrophysiological studies in rats describing an inhibitory GABAergic projection from CEl to CEm[13–17], we examined anatomical and functional connectivity between CEl and CEm. First, we locally injected a retrogradely tracing virus (herpes simplex virus 1 (HSV-1))[25] into CEl or CEm. Whereas injections into CEm resulted in intense retrograde labelling of neurons in CEl, CEm remained largely devoid of GFP after injections into CEl (Supplementary Fig. 5), indicating that CEl projects to CEm in a mostly unidirectional manner[26]. Next, to address whether identified CEl_{on} or CEl_{off} neurons project to CEm, we performed intracellular recordings in anaesthetized animals which were previously fear conditioned. Like in awake and behaving animals, CEl neurons recorded in anaesthetized mice were spontaneously active (Fig. 2d, e) and displayed both excitatory (5 of 12 neurons) and inhibitory (2 of 12 neurons) CS responses (Fig. 2d, e). Morphological reconstruction of neurobiotin-filled neurons revealed that the axons of both subtypes arborize locally within CEl, and send collaterals to CEm (Fig. 2d, e). To test whether CEl_{on} and CEl_{off} neurons functionally inhibit CEm neurons, we performed simultaneous multi-site single-unit recordings in CEl and CEm and cross-correlated spiking activity between identified pairs of neurons. Both CEl_{on} and CEl_{off} neurons exhibited inhibitory interactions with CEm neurons (Supplementary Fig. 6). No interactions in the reverse direction (from CEm to CEl) were found. These findings provide strong evidence that two distinct subclasses of CEl neurons inhibit CEm neurons *in vivo* (Fig. 2f). Considering that CEl_{on} and CEl_{off} neurons exhibited opposite changes in CS-evoked firing during fear conditioning, this raises the question of whether at the level of CEm output neurons fear conditioning results in CS-evoked inhibition or disinhibition.

To address this, we identified CEm output neurons by placing a stimulation electrode in the mesencephalic axon bundle, a fibre tract containing CEm projections to brainstem targets[9]. In four out of six cases, reliable time-locked antidromic responses could be evoked under anaesthesia after identification of neuronal responses in CEm units in freely moving fear-conditioned mice (Fig. 3a, b). Consistent with the finding that unconditioned freezing can be induced by activation of CEm or by inhibition of CEl, 83% of neurons located in CEm exhibited a marked increase in CS^+-evoked firing 24 h after fear conditioning (Fig. 3c), including all four identified brainstem-projecting CEm cells. The remainder of the units did not exhibit any CS^+-evoked responses. Like in CEl, CS responses of CEm output neurons started to change during fear conditioning and discriminated between CS^+ and CS^- (unpaired control stimulus) presentations (Supplementary Fig. 7). CEm neurons displayed a bi-phasic CS response (Supplementary Fig. 7). The first component was brief with a short (10–15 ms) onset latency similar to excitatory CS responses of CEl_{on} neurons. The second component was more sustained, paralleling the time course of inhibitory CEl_{off} responses, albeit with a slightly longer onset latency (Supplementary Fig. 7). These findings are consistent with the notion that conditioned CS responses of CEm output neurons reflect the integration of both excitatory and disinhibitory inputs (see circuit scheme in Supplementary Fig. 8).

Tonic inhibition and fear generalization

Given that CEm output is under tonic inhibitory control from CEl, this raises the question as to whether spontaneous activity in CEl and

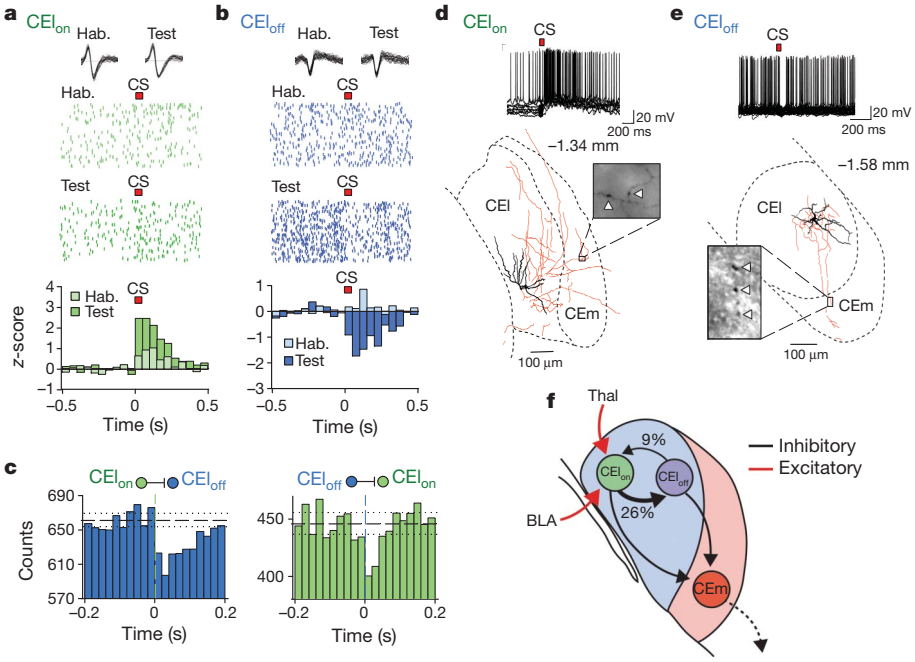

Figure 2 | Fear conditioning induces cell-type-specific plasticity in CEl inhibitory circuits. **a**, **b**, A subpopulation of CEl units (CEl$_{on}$ neurons) exhibited an increase in CS-evoked firing after fear conditioning (**a**), whereas another subpopulation (CEl$_{off}$ neurons) acquired an inhibitory CS response (**b**). Example raster plots (top) and normalized and averaged population peri-stimulus time histograms (PSTHs; bottom) from all CEl$_{on}$ or CEl$_{off}$ units, respectively, are shown, illustrating fear conditioning-induced changes in CS-evoked firing. The duration of the auditory stimulus is indicated (red bar; CS). Traces show superimposed spike waveforms recorded during habituation and test, respectively. **c**, Asymmetric functional organization of local inhibitory circuits in CEl. Left panel: averaged cross-correlation analysis ($n = 9$ pairs) illustrating a short latency inhibitory interaction between CEl$_{on}$ and CEl$_{off}$ neurons in 26% of all recorded pairs. Dashed vertical line indicates time of reference spikes from CEl$_{on}$ units. Right panel: averaged cross-correlation analysis ($n = 3$ pairs) illustrating a short latency inhibitory interaction between CEl$_{off}$ and CEl$_{on}$ neurons in 9% of all recorded pairs. Dashed horizontal line indicates mean; dotted lines indicate 95% confidence interval. **d**, **e**, CEl$_{on}$ and CEl$_{off}$ neurons send axon collaterals to CEm. Top: example intracellular recordings of a CEl$_{on}$ and a CEl$_{off}$ neuron spontaneously active at resting membrane potential (V_m). CS presentation induced an increase (in CEl$_{on}$ neurons) or a decrease (in CEl$_{off}$ neurons) in firing. Bottom: reconstruction of the neurobiotin-filled neurons revealed extensive local axonal branching and projections targeting CEm. Soma and dendrites are indicated in black, axon is shown in red. Inset shows putative synaptic contacts as suggested by the presence of axonal boutons in CEm (arrowheads). Numbers indicate the antero-posterior coordinates caudal to bregma. **f**, Schematic illustrating the organization of CEA inhibitory circuits based on electrophysiological and morphological data. Statistical analysis is shown in the Supplementary Information. Thal., Thalamus.

CEm is subject to regulation, and how plasticity of spontaneous activity might contribute to the encoding of conditioned fear responses. Indeed, spontaneous activity of CEm output neurons was markedly decreased after fear conditioning (Fig. 4a). Conversely, CEl$_{off}$ neurons exhibited increased spontaneous activity after fear conditioning, whereas on average CEl$_{on}$ neurons showed a slight decrease (Fig. 4a).

Phasic z-scored CS-evoked neuronal activity was highly correlated with freezing behaviour in all three neuronal subpopulations (Fig. 4b and Supplementary Fig. 9). However, because z-scores reflect CS-evoked neuronal activity normalized to pre-CS tonic activity, an increase in the z-score could reflect a net increase in the phasic (for example, synaptic) CS response, or a decrease in the absolute level or in the variability of pre-CS tonic activity. Plotting changes in tonic versus changes in phasic activity revealed that the two phenomena were correlated (Supplementary Fig. 10). However, plasticity of phasic and tonic activity seem to be independent processes, as fear conditioning did not affect variability of tonic activity and also increased phasic CS responses in neurons that did not exhibit concomitant changes in tonic activity (Supplementary Fig. 10).

What might be the behavioural relevance of plasticity of tonic activity in CEA inhibitory circuits? After fear conditioning, absolute and z-scored levels of tonic activity were only poorly correlated with freezing (Fig. 4c and Supplementary Fig. 11). Fear-conditioning-induced changes in tonic activity were not limited to periods of CS^+ exposure, but were also manifest during CS^- stimulation (Supplementary Fig. 12), indicating that plasticity of tonic activity could regulate the signal-to-noise ratio by linearly offsetting both CS^+- and CS^--evoked phasic responses. This would be expected to affect fear generalization. Consistent with this notion, changes in tonic activity predicted CS^+ versus CS^- discrimination at the behavioural level (Fig. 4d). Specifically, a decrease in tonic activity of CEm output neurons was associated with generalization, whereas CEl$_{off}$ neurons and CEl$_{on}$ neurons exhibited the inverse correlation (Fig. 4d and Supplementary Fig. 8), consistent with tonic inhibition of CEm output neurons by both CEl$_{on}$ and CEl$_{off}$ neurons. In addition, a receiver operating characteristic analysis (ROC) of the pooled CEl population revealed that changes in tonic activity of CEl neurons were significantly higher ($P < 0.01$) in generalizing mice compared to discriminating ones. Notably, changes in tonic activity were already present before CS onset (Supplementary Fig. 13), indicating that generalization is associated with a different functional network state, and that the stimulus specificity of conditioned fear responses is regulated by concerted changes in tonic and phasic activity within the neuronal circuitry of the CEA.

Discussion

Using targeted and reversible pharmacological and optogenetic approaches, we show that conditioned and unconditioned freezing behaviour is driven by CEm output neurons which are under tonic inhibitory control originating in CEl. Moreover, our study identifies CEl as an essential component of the neuronal circuitry underlying the acquisition of conditioned fear. We found that CEl contains two functionally distinct subpopulations of neurons forming highly organized local inhibitory circuits which inhibit CEm output neurons. Notably, an accompanying study[27] shows that at least one of these functionally defined subpopulations of CEl neurons (CEl$_{off}$ neurons) largely overlaps with a genetically defined neuronal subtype (PKC-δ^+ neurons). Our data indicate that whereas conditioned fear responses are driven

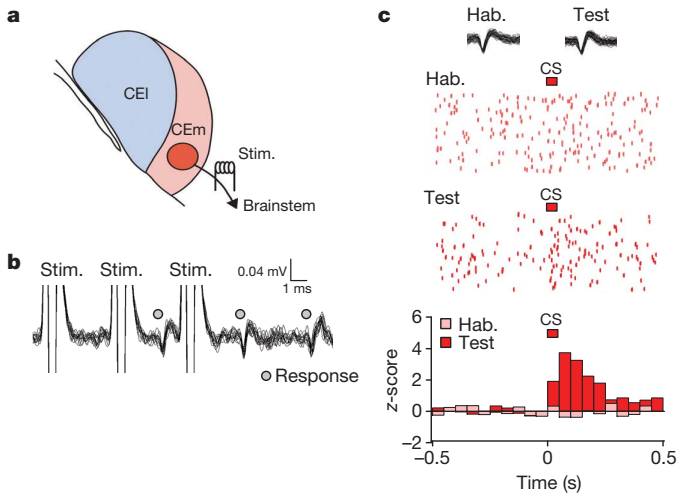

Figure 3 | Fear conditioning induces disinhibition of CEm output neurons. **a**, Identification of CEm output neurons by stimulation of the mesencephalic axon bundle. **b**, Stimulation of the mesencephalic axon bundle elicits antidromic spikes which exhibited low temporal jitter (<0.1 ms), and followed high-frequency (200 Hz) stimulation. **c**, CEm units exhibited an increase in CS-evoked firing after fear conditioning. Example raster plots (top) and normalized and averaged population PSTHs (bottom) from all CEm units illustrating fear-conditioning-induced changes in CS-evoked firing. The duration of the auditory stimulus is indicated (red bar; CS). Traces show superimposed spike waveforms recorded during habituation and test, respectively. Statistical analysis is shown in Supplementary Information.

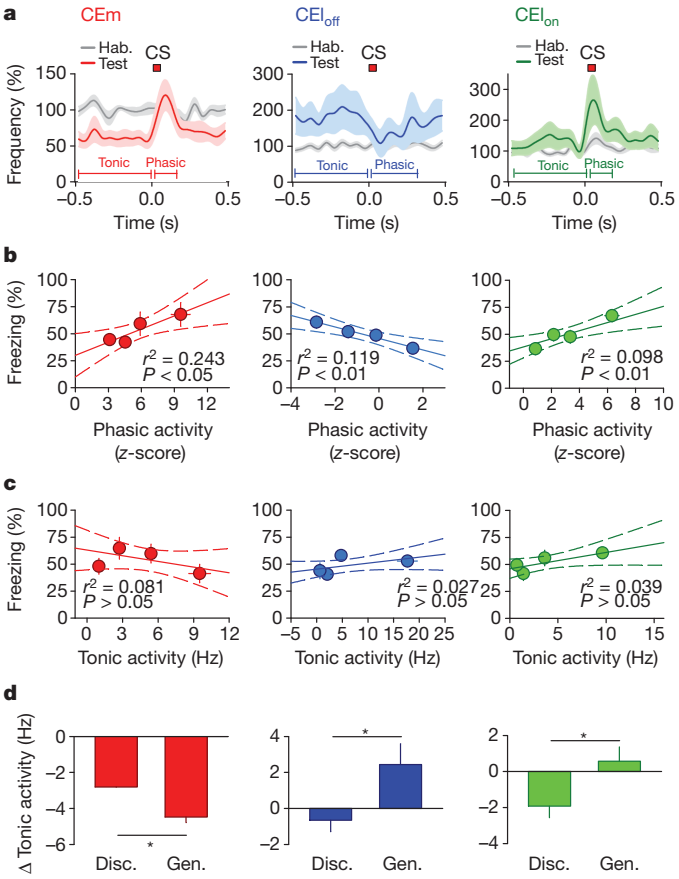

Figure 4 | Cell-type-specific plasticity of tonic activity regulates fear generalization. **a**, Normalized population PSTHs of CEm (left), CEl$_{off}$ (middle) and CEl$_{on}$ neurons (right). Fear conditioning was associated with decreased tonic activity in CEm and CEl$_{on}$ neurons, and increased tonic activity in CEl$_{off}$ neurons. Shaded area indicates s.e.m. **b**, Phasic z-scored CS responses of CEm (left), CEl$_{off}$ (middle) and CEl$_{on}$ neurons (right) are correlated with freezing behaviour. Correlations were obtained by plotting the averaged z-scored responses for all neurons of a given subtype for each animal over blocks of two CSs. Plots include both CS$^+$ and CS$^-$ responses. Data were averaged and binned (bins contain an equal number of data points). Linear correlations were performed using the non-binned raw data (Supplementary Fig. 9). P values indicate significance levels of Pearson's correlation coefficients. Dashed lines indicate 95% confidence intervals. All error bars indicate mean ± s.e.m. **c**, Tonic activity does not correlate with freezing behaviour. **d**, Cell-type-specific plasticity of tonic activity predicts fear generalization. Changes in tonic activity were different when animals exhibited CS$^+$/CS$^-$ discrimination (Disc.; freezing ratio CS$^+$/CS$^-$ > 1.4) or when animals generalized (Gen.; freezing ratio CS$^+$/CS$^-$ < 1.4). Whereas CEm units showed a stronger decrease in tonic activity upon generalization, CEl$_{off}$ neurons and CEl$_{on}$ neurons exhibited the inverse correlation. *P < 0.05. Statistical analysis is shown in the Supplementary Information.

by CS-evoked disinhibition of CEm output neurons, cell-type-specific plasticity of tonic inhibitory network activity within the CEl/CEm circuitry regulates generalization of conditioned fear responses.

Inactivation of CEl during the acquisition of fear conditioning interfered with learning. This suggests a role for synaptic plasticity at glutamatergic inputs onto CEl$_{on}$ neurons during fear conditioning. CEl receives glutamatergic input from various brain structures including the basolateral complex of the amygdala (BLA), insular cortex, and brainstem, in particular from the parabrachial nucleus[12]. Afferents originating from the parabrachial nucleus make very strong and reliable synapses onto CEl neurons[28], and might function as a teaching signal enabling the induction of synaptic plasticity at other inputs. However, although long-term potentiation can be induced at various inputs to the CEl in slice preparations[29,30], the role of specific afferent pathways in fear conditioning remains to be determined.

After fear conditioning, CEm output neurons exhibited CS-evoked bi-phasic excitation, consisting of a brief short-latency response followed by a slower second component. Considering the very short onset latency of the first component (less than 15 ms) it is likely to be driven by direct excitatory input from auditory thalamic nuclei[12,22,23,31]. Because CEl$_{on}$ neurons also exhibited short-latency excitatory responses, thalamo-CEm excitation may be terminated by feedforward inhibition through the CEl$_{on}$ pathway. Consistent with this scenario, sparse inputs from auditory thalamus (suprageniculate and posterior intralaminar nuclei) to the capsular part of CEl have been described[24]. Alternatively, termination of short-latency responses might also reflect feedforward inhibition mediated by intercalated cell clusters (ITCs)[32,33]. The observation that short-latency excitation of CEm output neurons increased with fear conditioning indicates that thalamo-CEm synapses might be strengthened, possibly involving NMDA receptor-dependent long-term potentiation[30].

The second component of CS-evoked responses of CEm output neurons, which had a much longer duration and contained most of the spikes, most likely reflects disinhibitory input from CEl, and possibly from nearby ITCs[34] as well as direct excitatory input from BLA. Several arguments support a role for disinhibition via the CEl$_{off}$ pathway. First, CEl$_{off}$ neurons can project to CEm, functionally inhibit CEm output neurons and regulate conditioned freezing behaviour (see also the accompanying paper[27]). Second, pharmacological inactivation of CEl induced CEm-dependent freezing behaviour, demonstrating that CEm is under tonic inhibitory control from CEl. Third, CS-evoked inhibition of CEl$_{off}$ neurons started right before the onset of slow excitation in CEm. Moreover, CS responses of CEl$_{off}$ and CEm units exhibited a similar time course, which was much slower than excitatory CS responses of BLA neurons under comparable conditions[21]. Finally, pharmacological inactivation of CEl during fear conditioning resulted in a learning deficit, indicating that activity-dependent plasticity of CEl to CEm signalling is necessary for the acquisition of conditioned fear responses. Together, these findings strongly indicate that disinhibition

through the CEl_{off} pathway contributes to fear-conditioning-induced changes in CEm output.

Fear conditioning induced cell-type-specific plasticity of tonic activity. Strong decreases in tonic activity of CEm neurons, or increases in tonic activity of CEl_{off} neurons, predicted generalization of behavioural responses to the CS^-. Previous studies have implicated auditory cortex or cortico-LA connections in stimulus discrimination and fear generalization[35–37]. However, because the CEA is downstream of auditory cortex and the LA, regulation of fear generalization in the CEA might override stimulus discrimination established in these upstream structures. This would enable animals to re-adjust the appropriate degree of fear generalization according to internal state and environmental demands.

Our results are consistent with studies on appetitive conditioning paradigms[38,39] indicating that CEA can process fear-related information in series with the BLA, or independently, in a parallel manner. In a serial processing mode, inhibitory circuits in the CEA may further select instructive signals sent out by the BLA, thereby increasing the computational power and the possibilities for modulation of the amygdala circuitry. In addition, the CEA might function in parallel with, or even independently of, BLA and directly elicit conditioned or unconditioned emotional behaviours in response to specific internal states associated with altered neuromodulatory input, such as chronic pain[40]. Interestingly, CEA output has also been suggested to exert strong control over basal forebrain cholinergic circuits[41,42], indicating that the CEA also affects processing in higher brain structures like the neocortex.

Our data reveal that inhibitory circuits in the CEA are highly organized, and establish important, but distinct, roles for plasticity of phasic and tonic inhibitory network activity in fear conditioning. Inhibitory circuits, such as those in striatum, have been proposed to be particularly effective in output selection based on winner-share-all mechanisms[43]. Thus, CEA inhibitory circuits may fine-tune and select output pathways targeting distinct downstream structures depending on the pattern of afferent synaptic input and local neuromodulatory activity. Given that CEA circuitry is thought to be organized similarly to striatal circuits[15], this may indicate that coordinated changes in phasic and tonic inhibition are a widespread mechanism regulating stimulus specificity of associative learning in the CNS.

METHODS SUMMARY

Behaviour and pharmacological inactivations. Mice were submitted to a discriminative auditory fear conditioning paradigm in which the CS^+, but not the CS^-, was paired with an US (mild foot shock). Freezing behaviour was quantified using an automatic infrared beam detection system as previously described[21]. Bilateral inactivation of the CEA or CEA subdivisions was achieved using microiontophoretic injection of fluorescently labelled muscimol before fear conditioning or retrieval test. Behavioural discrimination was analysed using clustering and ROC analyses as described (see Methods).

Electrophysiological recordings and analysis. Individual neurons were recorded extracellularly in freely behaving mice. Spikes of individual neurons were sorted by time-amplitude window discrimination and template matching as previously described[21,44]. Cluster quality was verified by quantifying the cluster separation[44] (Supplementary Fig. 14). Unit isolation was verified using auto- and cross-correlation histograms. Spike rasters and histograms were constructed by aligning sweeps relative to the CS onset, and CS-evoked responses were normalized to baseline activity using a *z*-score transformation.

Virus injections and optical stimulation. Animals were stereotaxically injected with an AAV serotype 2/7 expressing ChR22A-tdimer. Behavioural experiments were performed after 4 weeks of recovery and expression time and 3 days of handling. Optic fibres with a diameter of 200 μm were inserted into chronically implanted guide cannulae. ChR2-expressing cells were stimulated using a 473-nm laser. Freezing with and without light stimulation was quantified as described above.

Intracellular recordings and morphological reconstructions. Intracellular recordings were obtained from head-fixed animals under chloral hydrate anaesthesia (400 mg kg^{-1}) using standard methods. After completion of the recordings, animals were transcardially perfused and the brain kept for morphological reconstruction of the neurobiotin-filled recorded neurons.

Full Methods and any associated references are available in the online version of the paper at www.nature.com/nature.

Received 23 February; accepted 7 October 2010.

1. LeDoux, J. E. Emotion circuits in the brain. *Annu. Rev. Neurosci.* **23,** 155–184 (2000).
2. Davis, M. The role of the amygdala in conditioned and unconditioned fear and anxiety. In *The Amygdala* (ed., Aggleton, J. P.) 213–288 (Oxford Univ. Press, 2000).
3. Maren, S. & Quirk, G. J. Neuronal signalling of fear memory. *Nature Rev. Neurosci.* **5,** 844–852 (2004).
4. Sigurdsson, T., Doyère, V., Cain, C. K. & LeDoux, J. E. Long-term potentiation in the amygdala: a cellular mechanism of fear learning and memory. *Neuropharmacology* **52,** 215–227 (2007).
5. Sah, P., Westbrook, R. F. & Lüthi, A. Fear conditioning and long-term potentiation: what really is the connection? *Ann. NY Acad. Sci.* **1129,** 88–95 (2008).
6. Krettek, J. E. & Price, J. L. A description of the amygdaloid complex in the rat and cat with observations on intra-amygdaloid axonal connections. *J. Comp. Neurol.* **178,** 255–279 (1978).
7. Veening, J. G., Swanson, L. W. & Sawchenko, P. E. The organization of projections from the central nucleus of the amygdala to brainstem sites involved in central autonomic regulation: a combined retrograde transport-immunohistochemical study. *Brain Res.* **303,** 337–357 (1984).
8. LeDoux, J. E., Iwata, J., Cicchetti, P. & Reis, D. J. Different projections of the central amygdaloid nucleus mediate autonomic and behavioral correlates of conditioned fear. *J. Neurosci.* **8,** 2517–2529 (1988).
9. Pascoe, J. P. & Kapp, B. S. Electrophysiological characteristics of amygdaloid central nucleus neurons during Pavlovian fear conditioning in the rabbit. *Behav. Brain Res.* **16,** 117–133 (1985).
10. Goosens, K. A. & Maren, S. Pretraining NMDA receptor blockade in the basolateral complex, but not the central nucleus, of the amygdala prevents savings of conditional fear. *Behav. Neurosci.* **117,** 738–750 (2003).
11. Wilensky, A. E., Schafe, G. E., Kristensen, M. P. & LeDoux, J. E. Rethinking the fear circuit: the central nucleus of the amygdala is required for the acquisition, consolidation, and expression of Pavlovian fear conditioning. *J. Neurosci.* **26,** 12387–12396 (2006).
12. Samson, R. D., Duvarci, S. & Paré, D. Synaptic plasticity in the central nucleus of the amygdala. *Rev. Neurosci.* **16,** 287–302 (2005).
13. Ehrlich, I. *et al.* Amygdala inhibitory circuits and the control of fear memory. *Neuron* **62,** 757–771 (2009).
14. Sun, N., Yi, H. & Cassell, M. D. Evidence for a GABAergic interface between cortical afferents and brainstem projection neurons in the rat central extended amygdala. *J. Comp. Neurol.* **340,** 43–64 (1994).
15. Cassell, M. D., Freedman, L. J. & Shi, C. The intrinsic organization of the central extended amygdala. *Ann. NY Acad. Sci.* **877,** 217–241 (1999).
16. Veinante, P. & Freund-Mercier, M. J. Branching patterns of central amygdaloid nucleus afferents in the rat: Single axon reconstructions. *Ann. NY Acad. Sci.* **985,** 552–553 (2003).
17. Huber, D., Veinante, P. & Stoop, R. Vasopressin and oxytocin excite distinct neuronal populations in the central amygdala. *Science* **308,** 245–248 (2005).
18. Roberto, M., Madamba, S. G., Moore, S. D., Tallent, M. K. & Siggins, G. R. Ethanol increases GABAergic transmission at both pre- and postsynaptic sites in rat central amygdala neurons. *Proc. Natl Acad. Sci. USA* **100,** 2053–2058 (2003).
19. Gradinaru, V. *et al.* Targeting and readout strategies for fast optical neural control *in vitro* and *in vivo*. *J. Neurosci.* **27,** 14231–14238 (2007).
20. Tang, W. *et al.* Faithful expression of multiple proteins via 2A-peptide self-processing: A versatile and reliable method for manipulating brain circuits. *J. Neurosci.* **29,** 8621–8629 (2009).
21. Herry, C. *et al.* Switching on and off fear by distinct neuronal circuits. *Nature* **454,** 600–606 (2008).
22. LeDoux, J. E., Ruggiero, D. A. & Reis, D. J. Projections to the subcortical forebrain from anatomically defined regions of the medial geniculate body in the rat. *J. Comp. Neurol.* **242,** 182–213 (1985).
23. Turner, B. H. & Herkenham, M. Thalamoamygdaloid projections in the rat: a test of the amygdala's role in sensory processing. *J. Comp. Neurol.* **313,** 295–325 (1991).
24. Linke, R., Braune, G. & Schwegler, H. Differential projection of the posterior paralaminar thalamic nuclei to the amygdaloid complex in the rat. *Exp. Brain Res.* **134,** 520–532 (2000).
25. Lima, S. Q., Hromadka, T., Znamenskiy, P. & Zador, A. M. PINP: a new method of tagging neuronal populations for identification during *in vivo* electrophysiological recording. *PLoS ONE* **4,** e6099 (2009).
26. Pitkänen, A., Savander, V. & LeDoux, J. E. Organization of intra-amygdaloid circuitries in the rat: an emerging framework for understanding functions of the amygdala. *Trends Neurosci.* **20,** 517–523 (1997).
27. Haubensak, W. *et al.* Genetic dissection of an amygdala microcircuit that gates conditioned fear. *Nature* doi:10.1038/nature09553 (this issue).
28. Delaney, A. J., Crane, J. W. & Sah, P. Noradrenaline modulates transmission at a central synapse by a presynaptic mechanism. *Neuron* **56,** 880–892 (2007).
29. Fu, Y. & Shinnick-Gallagher, P. Two intra-amygdaloid pathways to the central amygdala exhibit different mechanisms of long-term potentiation. *J. Neurophysiol.* **93,** 3012–3015 (2005).
30. Lopez de Armentia, M. & Sah, P. Bidirectional synaptic plasticity at nociceptive afferents in the rat central amygdala. *J. Physiol. (Lond.)* **581,** 961–970 (2007).
31. Samson, R. D. & Paré, D. Activity-dependent synaptic plasticity in the central nucleus of the amygdala. *J. Neurosci.* **25,** 1847–1855 (2005).
32. Millhouse, O. E. The intercalated cells of the amygdala. *J. Comp. Neurol.* **247,** 246–271 (1986).

33. Paré, D. & Smith, Y. The intercalated cell masses project to the central and medial nuclei of the amygdala in cats. *Neuroscience* **57,** 1077–1090 (1993).
34. Paré, D., Quirk, G. J. & LeDoux, J. E. New vistas on amygdala networks in conditioned fear. *J. Neurophysiol.* **92,** 1–9 (2004).
35. Thompson, R. F. The role of the cerebral cortex in stimulus generalization. *J. Comp. Physiol. Psychol.* **55,** 279–287 (1962).
36. Jarrell, T. W., Gentile, C. G., Romanski, L. M., McCabe, P. M. & Schneidermann, N. Involvement of cortical and thalamic auditory regions in retention of differential bradycardia conditioning to acoustic conditioned stimuli in rabbits. *Brain Res.* **412,** 285–294 (1987).
37. Shaban, H. *et al.* Generalization of amygdala LTP and conditioned fear in the absence of presynaptic inhibition. *Nature Neurosci.* **9,** 1028–1035 (2006).
38. Cardinal, R. N., Parkinson, J. A., Hall, J. & Everitt, B. J. Emotion and motivation: the role of the amygdala, ventral striatum, and prefrontal cortex. *Neurosci. Biobehav. Rev.* **26,** 321–352 (2002).
39. Balleine, B. W. & Killcross, S. Parallel incentive processing: an integrated view of amygdala function. *Trends Neurosci.* **29,** 272–279 (2006).
40. Neugebauer, V., Galhardo, V., Maione, S. & Mackey, S. C. Forebrain pain mechanisms. *Brain Res. Brain Res. Rev.* **60,** 226–242 (2009).
41. Jolkkonen, E., Miettinen, R., Pikkarainen, M. & Pitkänen, A. Projections from the amygdaloid complex to the magnocellular cholinergic basal forebrain in rat. *Neuroscience* **111,** 133–149 (2002).
42. Gozzi, A. *et al.* A neural switch for active and passive fear. *Neuron* **67,** 656–666 (2010).
43. Wickens, J. R., Arbuthnott, G. W. & Shindou, T. Simulation of GABA function in the basal ganglia: computational models of GABAergic mechanisms in basal ganglia function. *Prog. Brain Res.* **160,** 313–329 (2007).
44. Nicolelis, M. A. L. *et al.* Chronic, multisite, multielectrode recordings in macaque monkeys. *Proc. Natl Acad. Sci. USA* **100,** 11041–11046 (2003).

Supplementary Information is linked to the online version of the paper at www.nature.com/nature.

Acknowledgements We thank all members of the Lüthi laboratory for discussions and critical comments on the manuscript. This work was supported by grants from the Austrian Science Fund (FWF), the Swiss National Science Foundation, the Schering Foundation, the European Commission (Eurospin Project, Contract HEALTH-F2-2009-241498), the Indo Swiss Joint Research Programme, the BMBF (grant 01GQ0420 to BCCN Freiburg), Neurex Interreg-IV, the Volkswagen Stiftung, the Novartis Institutes for Biomedical Research, and the Novartis Research Foundation.

Author Contributions S.C. and C.H. initiated the project. S.C., C.H., F.G., S.B.E.W. and C.M. performed the experiments. S.C., C.H., F.G., S.B.E.W., I.V., M.B.S. and A.L. analysed the data. K.D. and R.S. provided constructs and advice. S.C., C.H., F.G., S.B.E.W., I.E. and J.J.L. contributed to the experimental design and interpretation. A.L. conceived the project, contributed to the experimental design and interpretation, analysed data and wrote the manuscript. S.C. and C.H. contributed equally. All authors discussed the results and commented on the manuscript.

Author Information Reprints and permissions information is available at www.nature.com/reprints. The authors declare no competing financial interests. Readers are welcome to comment on the online version of this article at www.nature.com/nature. Correspondence and requests for materials should be addressed to A.L. (andreas.luthi@fmi.ch).

METHODS

Animals. Male C57BL6/J mice (2–3 months old; Harlan Ltd) were individually housed for 7 days before all experiments, under a 12 h light/dark cycle, and provided with food and water ad libitum. All animal procedures were executed in accordance with institutional guidelines and were approved by the Veterinary Department of the Canton of Basel-Stadt.

Behaviour. Fear conditioning and fear test took place in two different contexts (context A and B). The conditioning and test boxes and the floor were cleaned with 70% ethanol or 1% acetic acid before and after each session, respectively. To score freezing behaviour, an automatic infrared beam detection system placed on the bottom of the experimental chambers (Coulbourn Instruments) was used. Mice were considered to be freezing if no movement was detected for 2 s and the measure was expressed as a percentage of time spent freezing. To ensure that our automatic system scores freezing rather than just immobility, we previously compared the values obtained with those measured using a classical time-sampling procedure during which an experimenter blind to the experimental conditions determined the mice to be freezing or not freezing every 2 s (defined as the complete absence of movement except for respiratory movements)[21]. The values obtained were 95% identical and the automatic detection system was therefore used throughout the experimental sessions. On day 1, mice were submitted to a habituation session in context B, in which they received 4 presentations of the CS^+ and the CS^- (total CS duration of 30 s, consisting of 50-ms pips repeated at 0.9 Hz, 2-ms rise and fall; pip frequency: 7.5 kHz or white noise, 80 dB sound pressure level). Discriminative fear conditioning was performed on day 2 by pairing the CS^+ with a US (1-s foot shock, 0.6 mA, 5 CS^+/US pairings; inter-trial interval: 20–180 s). The onset of the US coincided with the offset of the CS^+. The CS^- was presented after each CS^+/US association but was never reinforced (5 CS^- presentations, inter-trial interval: 20–180 s). The frequencies used for CS^+ and CS^- were counterbalanced across animals. On day 3, conditioned mice were submitted to fear retrieval in context B, during which they received four and four presentations of the CS^- and the CS^+, respectively. When plotting the evolution of the freezing response in relation to the CS presentation, we found that the freezing probability starts increasing around 1.3 s after the presentation of the first pip of the sequence (Supplementary Fig. 15). After the first two pip presentations, the probability of freezing has already sharply increased. These data are consistent with an equivalence of individual pips, justifying the analyses of electrophysiological responses at the level of individual pips. Pharmacological experiments were performed using a non-discriminative conditioning protocol.

US-induced flinching behaviour and vocalizations were compared in the presence and absence of muscimol in freely moving mice. Foot-shock amplitudes ranged from 0.1 to 1 mA (3-ms duration).

To classify the freezing behaviour we used an expectation-maximization algorithm that provided the maximum likelihood estimates for a gaussian mixture model (GMM). That is, given the two-dimensional behavioural data (CS^+ freezing, CS^- freezing) we estimated the probability density $f(x) \in F$ that is most likely to have generated the data. We assumed that the family F is a two-component mixture of Gaussian functions:

$$f(x;\theta) = \sum_{k=1}^{2} p_k \varphi(x; m_k, \sigma_k)$$

with

$$\varphi(x; m_k, \sigma_k) = \frac{1}{\sqrt{(2\pi)^D}\sigma_k} e^{-\frac{1}{2}\left(\frac{\|x-m_k\|}{\sigma_k}\right)^2}$$

where p_k are the mixing probabilities and m_k and σ_k are the mean and variance of the kth distribution, respectively. The number of dimensions is denoted by D ($D = 2$). The method yielded the parameters $\vartheta = (p_k, \mu_k, \sigma_k)$ that are most likely to have generated the data. We used a slightly higher threshold (discrimination: $CS^+/CS^- > 1.4$) than the one estimated by the expectation-maximization algorithm, to decrease the false positives and thus to have a more conservative estimate of the number of discriminating mice (Supplementary Fig. 16).

To test whether changes in tonic baseline firing rates of CEl neurons can predict generalization versus discrimination, we performed a receiver operating characteristic (ROC) analysis using the classification results of the behavioural data. The area under the ROC curve (AUC) had a value of 0.67, which is above chance level (0.5). To test significance of this value we computed AUC values for 1,000 surrogate samples, which were random permutations of the initial classification scheme. The results revealed significance ($P < 0.01$). Note, that significant results were also obtained using an equivalent Wilcoxon signed-rank test ($P < 0.01$). Thus, changes in tonic activity are a useful discriminator for freezing behaviour revealing that CEl neurons in generalizing mice exhibit higher changes (less negative and more positive) in tonic activity than CEl neurons in discriminating mice.

Surgery and single-unit recordings. Mice were anaesthetized with isoflurane (induction 5%, maintenance 2.5%) in O_2. Body temperature was maintained with a heating pad (CMA/150, CMA/Microdialysis). Mice were secured in a stereotaxic frame and unilaterally implanted in the amygdala with a multi-wire electrode aimed at the following coordinates: 1.3 mm posterior to bregma; ±2.9 mm lateral to midline; and 3.9 mm to 4.3 mm deep from the cortical surface. The electrodes consisted of 8–16 individually insulated nichrome wires (13 µm inner diameter, impedance 50–300 kΩ; California Fine Wire) contained in a 26-gauge stainless steel guide canula. The wires were attached to a 10 pin to 18 pin connector (Omnetics). The implant was secured using cyanoacrylate adhesive gel. After surgery mice were allowed to recover for 7 days. Analgesia was applied before and during the 3 days after surgery (Metacam). Electrodes were connected to a headstage (Plexon) containing eight to sixteen unity-gain operational amplifiers. The headstage was connected to a 16-channel computer-controlled preamplifier (gain ×100, band-pass filter from 150 Hz to 9 kHz, Plexon). Neuronal activity was digitized at 40 kHz and band-pass filtered from 250 Hz to 8 kHz, and was isolated by time–amplitude window discrimination and template matching using a Multichannel Acquisition Processor system (Plexon). At the conclusion of the experiment, recording sites were marked with electrolytic lesions before perfusion, and electrode locations were reconstructed with standard histological techniques.

Single-unit spike sorting and analysis. Single-unit spike sorting was performed using an Off-Line Spike Sorter (Plexon) as described[21,44,45] (Supplementary Fig. 14). Principal component scores were calculated for unsorted waveforms and plotted on three-dimensional principal component spaces, and clusters containing similar valid waveforms were manually defined. A group of waveforms was considered to be generated from a single neuron if it defined a discrete cluster in principal component space that was distinct from clusters for other units and if it displayed a clear refractory period (>1 ms) in the auto-correlogram histograms. In addition, two parameters were used to quantify the overall separation between identified clusters in a particular channel. These parameters include the J3 statistic, which corresponds to the ratio of between-cluster to within-cluster scatter, and the Davies–Bouldin validity index, which reflects the ratio of the sum of within-cluster scatter to between-cluster separation[44]. High values for the J3 and low values for the Davies–Bouldin validity index are indicative of good cluster separation. Control values for these statistics were obtained by artificially defining two clusters from the centred cloud of points in the principal component space from channels in which no units could be detected. Template waveforms were then calculated for well-separated clusters and stored for further analysis. Clusters of identified neurons were analysed offline for each recording session using principal component analysis and a template-matching algorithm. Only stable clusters of single units recorded over the time course of the entire behavioural training were considered.

To avoid analysis of the same neuron recorded on different channels, we computed cross-correlation histograms. If a target neuron presented a peak of activity at a time that the reference neuron fires, only one of the two neurons was considered for further analysis. CS-induced neural activity was calculated by comparing the firing rate after stimulus onset with the firing rate recorded during the 500 ms before stimulus onset (bin size, 50 ms; averaged over blocks of four CS presentations consisting of 108 individual sound pips in total) using a z-score transformation. Z-score values were calculated by subtracting the average baseline firing rate established over the 500-ms preceding stimulus onset from individual raw values and by dividing the difference by the baseline standard deviation. Classification of units was performed by considering a significant z-score value within 200 ms after CS onset during fear test. For statistical analysis, z-score comparisons were performed using the average z-score value calculated during the 100 ms after CS onset. Tonic activity at test was z-scored by calculating the average firing rate ±s.d. of 108 randomly chosen 500-ms sweeps during the pre-CS period and z-scoring tonic activity during the 500-ms pre-pip period to the pre-CS period. Results are presented as mean ± s.e.m.

To address CS-evoked latencies of the three CEA neuronal populations, normalized peri-stimulus time histograms (PSTH) were computed for each single neuron of each category using 5-ms bins. Population PSTHs were obtained by averaging single neuron PSTHs. CS-evoked onset latencies were calculated for the population PSTH based on the first significant bin (at least 2.5 s.d. of baseline activity).

To assess the significance of cross-correlograms during spontaneous activity between a reference and a target neuron, mean firing rate with 95% confidence limits of the target neuron was calculated. Short-latency inhibitory cross-correlograms were considered to be significant if the number of action potentials of the target neuron (−50 ms to 50 ms) was inferior to the 95% confidence limits. Furthermore, to show that the cross-correlograms were not simply occurring

by chance, the spike train of the target neuron was shuffled 100 times and a shuffled cross-correlogram was computed[46]. Absence of short-latency interaction in the shuffled cross-correlogram was indicative that the cross-correlations were not due to chance.

Muscimol iontophoresis. Muscimol microiontophoresis was performed in chronically implanted animals[21]. Single-barrel micropipettes with a tip diameter of 10 to 15 μm were cut at 1-cm length and filled with a solution containing muscimol covalently coupled to a fluorophore (Muscimol-Bodipy-TMR conjugated, Invitrogen; 5 mM in phosphate buffered saline (PBS) 0.1 M, DMSO 40%) or with bodipy alone (Invitrogen; 5 mM in PBS 0.1 M, DMSO 40%). Mice were bilaterally implanted at the following coordinates: 1.3 mm posterior to bregma; 2.9 mm lateral to midline; and 3.9 mm to 4.3 mm deep from the cortical surface. Chlorided silver wires were inserted in each micropipette and attached to a connector. A third silver wire screwed onto the skull and attached to the connector served as a reference electrode. The entire miniature was secured using cyanoacrylate adhesive gel. After surgery, mice were allowed to recover for 2 days. On the injection day, iontophoretic applications were performed by means of cationic current (+12 μA to +15 μA) for 15 min per side using a precision current source device (Stoelting). Mice were submitted to the behavioural procedure 5 min after the end of iontophoretic injections and were immediately perfused at the end of the experiments. Brains were collected for further histological analysis. Serial slices containing the amygdala were imaged at ×5 using an epifluorescence stereo microscope (Leica Microsystems), and the location and the extent of the injections were controlled. Statistical analyses were performed using paired and unpaired Student's *t*-test post-hoc comparisons at the $P < 0.05$ level of significance. Results are presented as mean ± s.e.m.

Intracellular recordings and morphological reconstructions. Intracellular recording sessions were done in mice under chloral hydrate anaesthesia (400 mg kg^{-1}), and ended the same day with the animal being transcardially perfused and the brain kept for morphological reconstruction of the neurobiotin-filled recorded neurons using standard methods[47]. During the experiment, the animal's head was held firmly by a holding bar cemented on the cranium. The absence of ear-bars allowed the use of an open-field speaker (ES1 Free Field Electrostatic Speaker, TDT) for auditory stimulation. Auditory responses of CEl neurons were determined by the presentation of tones of different frequencies (1–30 kHz) and intensities (using a RP2.1 processor and a HB7 headphone driver; TDT).

Intracellular electrodes were pulled from borosilicate glass tubing (1.5 mm outer diameter, 0.84 mm inner diameter; World Precision Instruments) using a Flaming-Brown micropipette puller (model P-97; Sutter Instruments). Electrodes were filled with 1.5% neurobiotin (Vector Laboratories Inc.) in 1 M potassium acetate. Impedances were measured *in situ* and ranged from 65 to 120 MΩ. Electrodes were slowly lowered in the brain via a micromanipulator (LN mini/combi; Luigs & Neumann). Recordings were acquired and analysed with ClampEx9.0 and ClampFit9.0 (Molecular Devices) through an intracellular recording amplifier (Axoclamp-2B, Molecular Devices) and a data digitizer (Digidata 1322A). Positive DC pulses (0.1–1.0 nA, 500 ms, 1 Hz) were used to eject neurobiotin into the neurons. Mice were then perfused transcardially with 4% paraformaldehyde in 0.1 M phosphate buffer. Brains were removed and stored in the perfusion fixative. They were later sliced on a microtome into 80-μm-thick sections and labelled for neurobiotin using the Vectastain Elite avidin–biotin complex peroxidase kit (Vector Laboratories Inc.). Neurons were reconstructed with the Neurolucida software (Microbrightfield).

Virus injections and optical stimulation. For optical activation of CEm output neurons, animals were injected into CEm with an AAV serotype 2/7 (Vector Core), containing a construct coding for ChR22A-tdimer[20] at −1.4 mm posterior and ±2.9 mm lateral to bregma at a depth of −4.4 mm. Briefly, deeply anaesthetized animals were fixed in a stereotactic frame (Kopf Instruments) and the skin above the skull was cut. Glass pipettes (tip diameter 10–20 μm), connected to a Picospritzer III (Parker Hannifin Corporation), were lowered by a Micropositioner (Kopf Instruments) to the depth of 4.4 mm. About 300 nl were pressure injected into CEm. In the same surgeries 26-gauge stainless steel guide cannulae (Plastics One) were implanted bilaterally along the same track above CEm at a depth of −3.9 mm. Guide cannulae were secured using cyanoacrylate adhesive gel (Henkel) and dental cement (Heraeus Dental). To prevent blockage of the cannulae, dummy cannulae (Plastics One) were inserted and fixed. Behavioural experiments were performed after 4 weeks of recovery and expression time and 3 days of handling. Dummy cannulae were removed and optic fibres with a diameter of 200 μm (Thorlabs GmbH) were inserted bilaterally into the implanted guide cannulae. Mice were then placed into a behavioural context and the optic fibres were connected to a blue laser ($\lambda = 473$ nm, 100 mW, Extreme Lasers). The mice received four 10-s pulses of blue light with intervals between 20 s and 60 s. Freezing with and without light stimulation was quantified as described. After the experiment, optic fibres were removed and animals were perfused for histological analysis of the injection site as described.

For retrograde tracing of projections, replication defective herpes simplex virus (HSV-1) (BioVex)[48] expressing eGFP was injected into either CEl (anteroposteriorly, −1.2 mm; laterality, −2.9 mm; depth, 4.1 mm) or CEm (see above). For identification of the injection site, the virus solution was mixed at 1:1,000 with blue fluorescing polymer microspheres (Duke Scientific Corp.). Before and after the surgery, systemic (Metacam, Boehringer Ingelheim) and local analgesic (Naropin, AstraZeneca AG) were administered. After 1 week of expression, animals were transcardially perfused with 4% PFA. The brain was removed and cut into 80 μm coronal slices. To improve the fluorescent signal, an immunostaining was performed. Slices were kept in blocking solution (3% BSA, 0.2% Triton in 0.1M PBS) for 1 h at room temperature, before application of the primary antibody (goat anti-GFP, Abcam; 1:500 in blocking solution) and incubated at 4 °C over night. After washing, slices were incubated with secondary antibody (Alexa Fluor 488, donkey anti goat, Invitrogen; 1:1,000 in PBS) at 4 °C over night. After a final wash, slices were mounted on cover slips and imaged.

45. Herry, C. *et al.* Processing of temporal unpredictability in human and animal amygdala. *J. Neurosci.* **27,** 5958–5966 (2007).
46. Fujisawa, S., Amarasingham, A., Harrison, M. T. & Buzsaki, G. Behavior-dependent short-term assembly dynamics in the medial prefrontal cortex. *Nature Neurosci.* **11,** 823–833 (2008).
47. Lang, E. J. & Paré, D. Synaptic and synaptically activated intrinsic conductances underlie inhibitory potentials in cat lateral amygdaloid projection neurons *in vivo*. *J. Neurophysiol.* **77,** 353–363 (1997).
48. Lima, S. Q., Hromadka, T., Znamenskiy, P. & Zador, A. M. PINP: a new method of tagging neuronal populations for identification during *in vivo* electrophysiological recording. *PLoS ONE* **4,** e6099 (2009).